Template-free routes to porous inorganic materials

Eric S. Toberer and Ram Seshadri

Received (in Cambridge, UK) 13th February 2006, Accepted 30th March 2006
First published as an Advance Article on the web 26th April 2006
DOI: 10.1039/b602153k

New approaches to solid-state reactivity have allowed us to develop unusual routes to porous inorganic materials. This article describes our recent work on template-free routes involving the selective leaching of one phase from a two-phase composite to form porous oxides. Subsequent reactions have been developed to yield porous metals, conformal coatings, and hierarchically porous materials. Pores can also be generated through simple redox processes in transition-metal oxides; such redox cycling allows mesopores to be produced in a regenerative process in a material which is already macroporous.

Introduction

The last two decades have seen great progress in the preparation of porous inorganic materials. New morphologies and chemical compositions are now achievable on a wide range of length scales. Beginning with the discovery of surfactant templated mesoporous materials in 1992 (MCM-41),[1] many new synthetic strategies have been realized. Pre-formed templates, self-assembling systems, and a variety of spontaneous processes have been used to induce porosity on the 1 nm to 10 μm length scale in extended inorganic systems.

The nature of the templates used to induce pores are themselves highly varied. They can be rigid and control porosity through partitioning of space, or in the case of structure-directing agents, by relying on differences in miscibility and the creation of chemical gradients as a means of inducing pores. For example, small amine molecules control the micropore (<2 nm) formation in zeolites, while surfactant assemblies[1] and more recently block copolymers[2] control the formation of mesoporous (2–50 nm) inorganic materials. Macroporous (>50 nm) inorganic materials have been formed through the lost wax casting of templates. In the formation of so-called macroporous inverse opals, assemblies of close-packed spheres are infiltrated with a variety of inorganic precursors, leading, after removal of template, to periodically porous inorganic materials.[3] Similarly, ordered emulsions have been used to template the formation of porous inorganic structures.[4,5] As the template morphology may be well-controlled, the resulting porosity is quite tuneable.

Porous inorganic materials are also found in the natural world. The tests of sea urchins are composed of calcite single crystals that grow in such a way that periodic pores are found that interpenetrate the calcite crystals.[6] Such structures are remarkable for their morphological and crystallographic control. Recently porous calcite single crystals that mimic sea urchin architectures have been prepared through controlled nucleation and templating.[7–9] Several other inorganic salts have also been formed as macroporous single crystals through these templating methods.[10] Sea urchin spines have also been used to template the formation of photonic structures.[11]

Hierarchically porous materials, displaying multiple length scales in pore size, are desirable for their improved flow performance coupled with high surface areas. Consequently, they have been the subject of much recent investigation. A multitude of wet chemistry routes to hierarchically porous

Materials Department and Materials Research Laboratory, University of California, Santa Barbara, CA, 93106, USA.
E-mail: etoberer@engineering.ucsb.edu; seshadri@mrl.ucsb.edu;
Fax: 1 805 893 8797; Tel: 1 805 893 6129

Eric Toberer

Eric S. Toberer was born in Eugene, Oregon in 1981. He earned his BS in Chemistry in 2002 from Harvey Mudd College in Claremont, California. Since September 2002, he has been pursuing a doctoral degree in the Materials Department at the University of California, Santa Barbara in the area of porous inorganic materials.

Ram Seshadri

Ram Seshadri is an Assistant Professor in the Materials Department at the University of California, Santa Barbara where he pursues interests in structure–property relations in inorganic materials (with an emphasis on magnetism), as well as in complex material architectures at various length scales.

inorganic materials have recently been developed. Combining structure-directing agents with templates such as latex spheres has enabled the formation of hierarchically porous structures that have porosity on the 10 and 100 nm length scales.[12] Zeolites have been grown within the confines of latex spheres, forming a macroporous structure, the walls of which are microporous.[13] Similarly, macroporous diatom structures have been used to template the growth of hierarchically porous zeolites.[14] An unusual group of hierarchically porous materials have been synthesized from alkoxide precursors which result in mesoporous walls composed of joined crystalline nanoparticles which are grown or assembled into walls of macroporous channels.[15,16] Tetramodal porosity with pore diameters ranging from 10 nm to 10 μm has been obtained from the assembly of silica nanoparticles on a porous organic template.[17]

Porous materials have also been formed through spontaneous, template-free methods, such as gas expulsion, dealloying, and selective leaching of one phase from a biphasic composite The release of carbon dioxide during the decomposition of dolomite has been used to induce porosity in the structural ceramic $CaZrO_3$.[18] Controlled evaporation of titanium sol similarly produces a volume loss which is expressed as a macropore network of titania.[19] Dealloying aluminium from an aluminium–nickel alloy leads to formation of the porous metal known as Raney nickel.[20] This leaching process has been extended to other systems and has been studied theoretically.[21]

Selective leaching of one phase from a composite has been used in the formation of a variety of porous glasses and ceramics. The formation of a two-phase composite may be achieved by physically mixing two immiscible phases and sintering the resulting material at high temperature to improve the strength of the resulting material. Immersion in an appropriate solution will dissolve out the sacrificial phase, leaving behind a porous monolith of the desired phase. Porosity and pore diameter may be adjusted by changing the starting phase ratio, particle diameter, and heat treatment. Additionally, solid-state reactions have been developed which result in two product phases, one of which is sacrificial. Crossing phase boundaries is one method of achieving two phases, as in the eutectic cooling of a melt to form two product phases. Suzuki has used such a reaction to form a composite of magnesia and zirconia, followed by removal of the magnesia phase to give porous zirconia.[22] Similarly, Vycor glass is formed through the spinodal decomposition of a borosilicate glass to borosilicate rich and borosilicate poor regions. The resulting composite is then rendered porous through acid leaching of the borosilicate rich phase.[23] Selective leaching to form macroporous materials has been applied to engineer fuel cells.[24] Composites of NiO and Y_2O_3-stabilized ZrO_2 (YSZ) were formed through tapecasting and firing. Reduction of the NiO phase to Ni and subsequently leaching in nitric acid led to macroporous sheets of YSZ with pores ranging from 1–5 μm in diameter.

In our work, the focus has been on selective leaching to form macroporous materials. Our general strategy has been to form an intimately mixed two-phase composite and then to leach out the sacrificial phase in solution (Fig. 1(a)), leaving a macroporous monolith of the desired phase. Thus far, we have formed bulk pellets of these materials, although the routes are amenable to other morphologies such as thin films. We have also developed several procedures for modifying the resulting macroporous material. Fig. 1(b) shows schematically the idiomorphic reduction of a macroporous oxide to a metal with the macropore structure being retained. A conformal coating of a second phase may also be developed on the pore walls through a process of reactive dip coating, as shown in Fig. 1(c). We have also formed hierarchically porous monoliths through the subsequent leaching of a sacrificial element from the macropore walls, leading to a macroporous material with mesoporous walls (Fig. 1(d)).

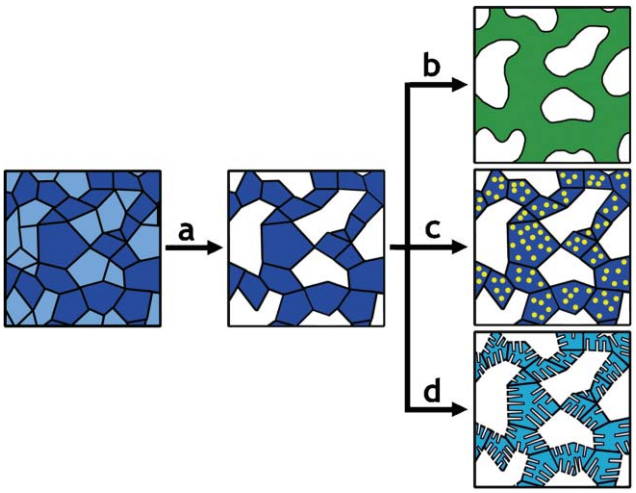

Fig. 1 Scheme showing (a) formation of a macroporous ceramic through selective leaching of a two-phase composite. The resulting material may then be (b) turned into a porous metal, (c) decorated with a conformal coating, or (d) rendered hierarchically porous through vapour-phase leaching.

Selective leaching

Our work on porous materials began with the selective leaching of a sacrificial phase from dense bulk composites. While routes such as templating had already achieved considerable success (see for example Newnham's seminal work on porous piezoelectrics which used coral as a template[25]), selective leaching had not yet achieved similar chemical complexity or morphological control in inorganic materials.

One attraction of selective leaching is that road maps already exist for the phase behavior, namely one simply needs look to the phase diagram that contains the sacrificial and desired phases and see if there is a two-phase region between them. We began with composites of rock salt NiO and wurtzite ZnO, as this mixture had several attractive features. First, ZnO is soluble in alkali solution while NiO is insoluble. Second, no ternary phases exist between the extreme NiO and ZnO phases. Third, the two-phase region is quite extensive both in temperature and composition; the two phases are largely immiscible but each can accommodate a small percentage of the other cation.

In forming a dense composite for selective leaching, care must be taken to ensure that the two phases are well mixed. The cross-section in Fig. 1(a) shows that the two phases are in intimate contact with one another. If instead the sacrificial phase were to agglomerate, large voids would form upon leaching. To form intimately mixed composites, we have had success with several techniques, including decomposition of precipitated hydroxy double salts,[26] combustion synthesis,[27] and decomposition of mixed metal oxalates.[28]

After initially forming an intimately mixed powder of the two phases, we have used uniaxial pressing to form pellets. Particle connectivity is then improved through firing at high temperature. A scanning electron micrograph of a cross-section of dense NiO–ZnO is shown in Fig. 2(a). The monolith shows virtually no pores, and the individual grains are well-connected to neighbouring grains. Elemental mapping of this cross-section with energy dispersive X-ray (EDX) analysis shows that the grains of each phase are randomly distributed and not agglomerated. Additionally, the grain sizes for the two phases are nearly identical. This characteristic is important if a pore structure with open connectivity is desired. A morphology composed of large grains of one phase surrounded by small grains of the other phase can lead to undesired effects on the monolith upon leaching. If the grains of the sacrificial phase are much larger than those of the desired phase, the resulting pores will be large and isolated. Conversely, if the grains of the desired phase are much larger than the sacrificial phase, no connectivity between the grains of the desired phase will exist, and upon leaching, the monolith will turn to a powder.

Leaching the NiO–ZnO composite results in macroporous NiO as shown in Fig. 2(b). Most importantly, the leaching has no effect on the NiO phase, and the connectivity of the NiO grains is maintained. The pore size of $\sim$1 μm agrees with the ZnO grain size from EDX mapping. As the pores are formed *via* leaching, they must be connected and do indeed appear continuous in the SEM.

The degree of porosity and the pore size may be tuned across a wide range. Adjusting the initial volume fraction of the sacrificial phase has a corresponding effect on the porosity. We have achieved average pore diameters between 500 nm and 5 μm with this method by adjusting the decomposition and sintering conditions.

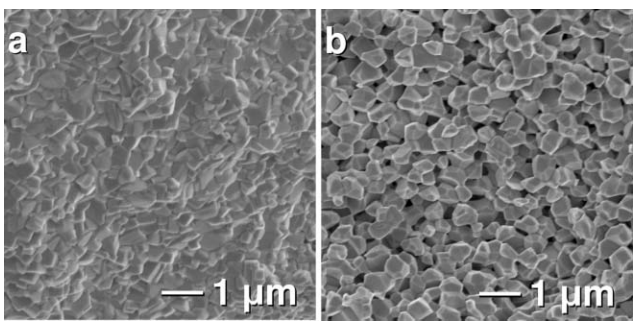

Fig. 2 Scanning electron microscope (SEM) images of (a) dense composite of NiO and ZnO phases, and (b) the resulting macroporous NiO that remains after alkali leaching.

Dense composites through metathesis

Solid state metathesis involves the exchange of ions from one phase for ions from another phase. This may be generally described as:

$$AB + CD \rightarrow AD + CB$$

Early work with solid-state metathetic reactions resulted in mixtures of LiCl and mixed metal ferrites.[29] The Kaner group has made the technique particularly well known by combining metathesis with self-propagation, forming powders ranging from ZrN and GaN to MoS_2.[30,31] We have previously looked at the formation of perovskites through reactions of the following type:

$$PbSO_4 + K_2CO_3 + TiO_2 \rightarrow PbTiO_3 + K_2SO_4 + CO_2\ (g)$$

We call this reaction "assisted metathesis", in that the transfer of the sulfate species drives the reaction forward.[32] Similar reactions can be used to form mixtures of $LaMnO_3$ and K_2SO_4.

Such reactions are amenable to selective leaching, as the sulfate is water soluble. Fig. 3(a) shows a SEM micrograph of a composite of $La_{0.7}Sr_{0.3}MnO_3$ and K_2SO_4 formed in this manner. Immersing the composite pellet in water completely removes the K_2SO_4 phase while leaving a macroporous monolith of $La_{0.7}Sr_{0.3}MnO_3$, as shown in Fig. 3(b).[33] In this manner, we have formed macroporous $PbTiO_3$, $LaMnO_3$ and $La_{0.7}Sr_{0.3}MnO_3$ with pores 1–10 μm in diameter and grains ranging from 0.5–5 μm. Leaching reveals that the necking between the perovskite grains is poor, but the strength may be improved by sintering the resulting porous material. The high temperature stability of these materials is demonstrated in Fig. 4, which shows a macroporous monolith of $LaMnO_3$ which was sintered at 1273 K for 48 h. While the grain connectivity has improved, the connected macropore network remains.

Concurrently with our work on porous perovskites, Gopalakrishnan and co-workers group have developed a large number of metathetic routes to perovskites oxides which produce a soluble salt as a second phase.[34] This emphasizes

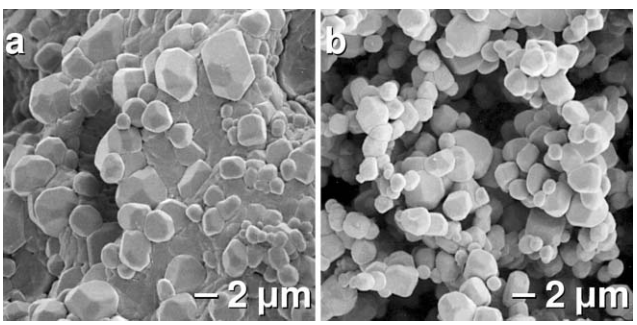

Fig. 3 SEM images showing (a) composite of $La_{0.7}Sr_{0.3}MnO_3$ and K_2SO_4 formed through a solid-state metathesis reaction and (b) macroporous $La_{0.7}Sr_{0.3}MnO_3$ formed through dissolution of the K_2SO_4 phase in water. Reproduced with permission from ref. 33. © 2004, American Chemical Society.

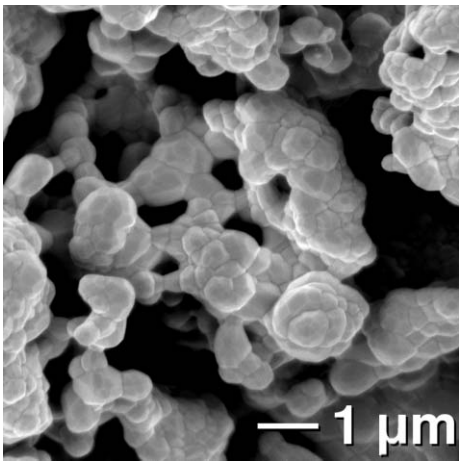

Fig. 4 SEM image of macroporous $LaMnO_3$ which was fired at 1273 K for 48 h. Significant necking between the grains has occurred, but the macropore network has not been compromised.

how general the technique is and the rich chemistry that ensues.

Subsequent reactivity

Once a porous monolith has been formed, a variety of subsequent reactions can be envisioned using liquid- or gas-phase reactants. We have used reactive dip coating to form conformal coatings of a second phase along the inner pore walls of NiO.[28] Dipping a NiO pellet in a concentrated solution of lanthanum acetate followed by drying and decomposition of the acetate leaves a coating of lanthanum oxide along the pore walls. Firing the resulting pellet at high temperature leads to a reaction between the pore walls and the coating, forming the $m = 3$ Ruddlesden–Popper phase $La_4Ni_3O_{10}$. Fig. 5 shows the resulting pore walls and the coating of $La_4Ni_3O_{10}$ sub-micron particles on the surface. This

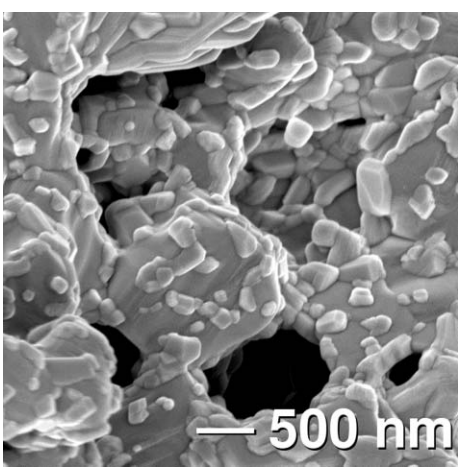

Fig. 5 Reactive dip coating reacts the macroporous support with a ion deposited from solution, leading to the formation of a complex oxide coating the inner surface. The material in the SEM image is composed of $La_4Ni_3O_{10}$ sub-micron particles coating the inner pore walls of a NiO monolith. Reproduced with permission from ref. 28. © 2005, American Chemical Society.

route should be contrasted with conventional dip coating, in which nanoparticles are deposited on an inert support. Instead, a stable, well-adhering coating of a complex ternary phase is obtained with a reactive support and high temperatures to promote diffusion.

Gas-phase reactions can also be used to alter the chemistry of the porous material. We have used a flowing 5% H_2/N_2 atmosphere to reduce porous monoliths of NiO and $ZnFe_2O_4$ to their metallic state.[28] Fig. 6 shows a cross-section of a porous pellet of Ni. The pore structure has been maintained, and the facetted nature of the original NiO structure has been smoothed out. Porous oxides appear to fracture at grain boundaries, whereas failure in the metals occurs through a ductile process, as seen in Fig. 6. For the reduction of $ZnFe_2O_4$, if the reduction was below the melting point of Zn (692.5 K), we obtained a monolith of $Zn_{0.3}Fe_{0.7}$, while at high temperatures (>900 K), zinc would be found deposited down stream at the edge of the furnace hot zone. A corresponding decrease in the concentration of Zn in the porous iron was observed.

Vapor-phase leaching

In both the nickel and iron cases described in the previous section, a significant volume loss occurs upon reduction to the metal. We have seen this volume loss express itself as smaller pores penetrating into the pore walls, although the sintering rates of the metals at the reduction temperatures are rapid enough that the mesopores are rather transient.[27]

Clearly, strategies for forming porous materials through volume loss need to involve temperatures where the pores that form are not rapidly closed. One option is to look for processes which result in oxides, not metals, since oxides do not sinter as rapidly. In the reduction of Mn_3O_4 to MnO, the volume loss is significant, and the process occurs at reasonably low temperatures in a flowing 5% H_2/N_2 atmosphere (reduction occurs around 725 K, whereas the melting point of MnO is 2113 K). We have formed pellets of macroporous Mn_3O_4 by simply pressing and firing a powder of Mn_3O_4 so that the grains developed some connectivity, but minimal densification

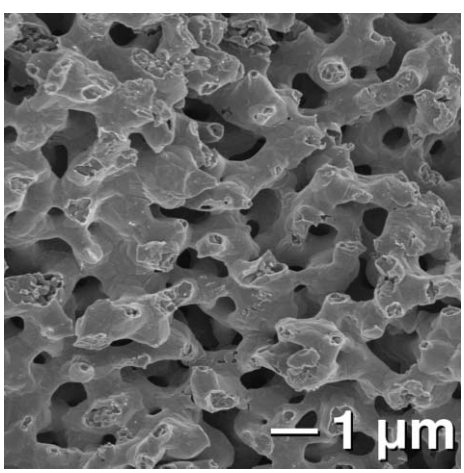

Fig. 6 SEM micrograph of a porous Ni monolith formed through reduction of macroporous NiO in a 5% H_2/N_2 atmosphere.

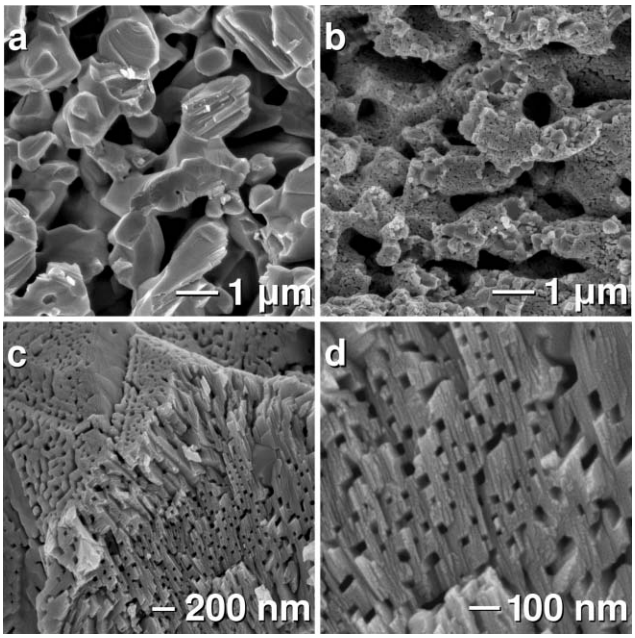

Fig. 7 (a) SEM micrograph of macroporous Mn_3O_4. (b) Upon reduction in a 5% H_2/N_2 atmosphere to MnO, the macropores are maintained and an additional level of porosity has been induced. The mesoporous fracture surface on the right side of image (c) is shown at higher magnification in micrograph (d).

occurred (Fig. 7(a)). As seen in Fig. 7(b), Mn_3O_4 pellets reduced to MnO maintain the macropore network and grain connectivity. Additionally, the volume loss inherent in the phase change results in mesopores penetrating into the macropore walls (Fig. 7(c)).[35] The macropores are 1 μm in diameter and the mesopores are 50 nm across. Unlike in the reduction to metallic Ni and Fe, the original grain facets are maintained, highlighting the difference in diffusivity. The resulting pores are rectangular and aligned across a grain, suggesting that crystallographic relations are controlling the pore orientation (Fig. 7(d)).

Reoxidation of hierarchically porous MnO to Mn_2O_3 closes the mesopores without altering the macropore network. Reduction of Mn_2O_3 back to MnO re-forms the mesopores in the macropore walls. As the pore forming process relies solely on strain due to a phase change with corresponding oxygen loss, the process may be cycled. Fig. 8 shows a MnO sample which has been through three redox cycles and continues to show pores on two different length scales. Some broadening of the mesopore size distribution is observed. To our knowledge, this is the first example of morphological regeneration of a porous material.[35] Such mesopore regeneration may prove to be useful in high temperature applications where sintering results in a loss of surface area.

In a manner similar to the leaching of Zn from $Zn_{0.3}Fe_{0.7}$ in a reducing atmosphere, $ZnMn_2O_4$ may also be reduced to rock salt $Zn_{0.3}Mn_{0.7}O$ and then converted to pure MnO through vapor-phase leaching.[36,37] When applied to dense pellets of $ZnMn_2O_4$, the material is rendered porous, with 50–200 nm pores penetrating throughout the MnO monolith (Fig. 9). By combining two distinct steps which individually give modest volume losses, namely a reductive phase transformation and

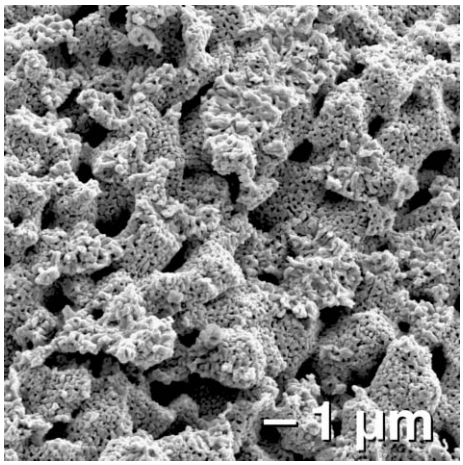

Fig. 8 Hierarchically porous MnO after three redox cycles continues to show pores on the 1 μm and 50 nm length scale.

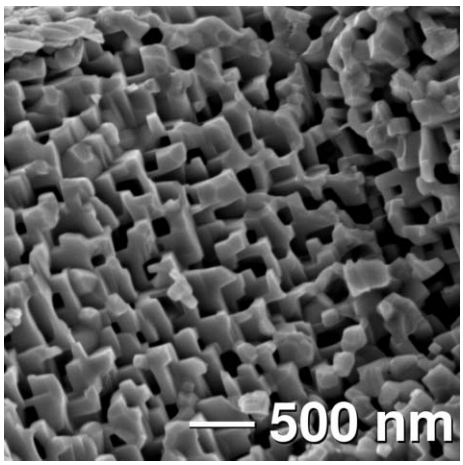

Fig. 9 SEM micrograph of porous MnO formed through the reduction and leaching of dense $ZnMn_2O_4$ in a 5% H_2/N_2 atmosphere. Reproduced with permission from ref. 37. © 2006, American Chemical Society.

the vapor-phase leaching of zinc, a material with significant porosity is obtained.

Macroporous $ZnMn_2O_4$ was formed by leaching ZnO from a dense composite of ZnO and $ZnMn_2O_4$. Reduction to rock salt and vapor-phase leaching of the zinc in a flowing 5% H_2/N_2 atmosphere produces mesopores in the macropore walls. The resulting hierarchically porous monolith of MnO is shown in Fig. 10. The fracture surface visible on the upper right of (a) is shown at higher magnification in (b) and is composed of aligned rectangular pores. The pore morphology is similar to that obtained from the reduction of Mn_3O_4, with an average diameter of 50 nm. Nitrogen sorption measurements were used to further characterize the pores. Fig. 11(a) shows the volume of nitrogen adsorbed as a function of partial pressure. Some hysteresis is observed at high partial pressures, indicative of the filling of large mesopores. From the adsorption, the pore size distribution was extracted using the Barrett–Joyner–Halenda (BJH) method. Fig. 11(b) shows that the mesopores have an average pore diameter of 50 nm and

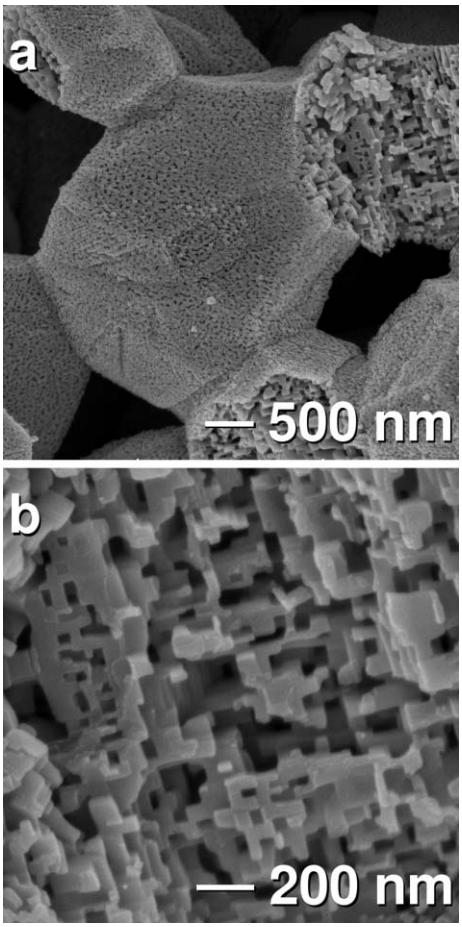

Fig. 10 SEM micrographs of hierarchically porous MnO monolith composed of macroporous walls which are themselves mesoporous. The fracture surface in the upper right of image (a) is shown at higher magnification in image (b). The mesopores are rectangular and aligned within each grain. (a) Reproduced with permission from ref. 37. © 2006, American Chemical Society. (b) Reproduced with permission from ref. 36. © 2006, Wiley–VCH.

general range between 20 and 100 nm. The tail of the macropore peak is present at 250 nm, but the full macropore peak is not revealed due to limitations of the technique.

The rectangular and aligned nature of the mesopores suggests that the pore morphology is crystallographically controlled. To determine this relationship, transmission electron microscopy (TEM) was performed on a 50 nm thick specimen.[37] A hierarchically porous pellet of MnO was backfilled with epoxy and polished down, and a lamella was formed with a focused ion beam (FIB). Fig. 12(a) shows part of the lamella formed by the FIB. The contrast variations across each grain are caused by density variations due to the pores. Using a selected area aperture and aligning on a zone axis, it was possible to determine that the samples were composed of crystalline grains 300–1000 nm in diameter. Fig. 12(b) shows a diffraction pattern obtained from the single crystallite in the left of the image. By tilting the sample into the [100] zone axis, we end up looking directly down the pores. Additionally, overlaying the diffraction pattern on the image shows that the <100> directions are normal to the faces of the pore walls. Thus, the pores are oriented along the <100> family of directions and the pore walls are composed of {100} crystal faces. These rectangular pores arise from the {100} faces being the lowest energy surfaces for the rocksalt lattice. For the sample shown, the Zn vapor-phase leaching was not complete, and a superlattice, perhaps associated with cation order, is visible in the TEM diffraction patterns.

It is important to emphasize that the hierarchically porous structures we obtain are composed of macropore walls which are made of mesoporous single crystals. Porous single crystals are extremely unusual and show potential for improved performance over their polycrystalline analogs due to the absence of grain boundaries. For high temperature applications, porous single crystals are significantly more stable due to lowered surface energies and the elimination of grain boundaries as the primary means of mass transport. Electrical transport is improved due to the absence of grain boundary scattering. In nature, sea urchins form spines of porous calcite single crystals.[6] Prior synthetic efforts to form porous single crystals have either used controlled nucleation within a porous template[7,9] or etching of a bulk single crystal.[38] In contrast, we have found that pores may be induced in crystalline grains through controlled phase changes that result in a volume loss.

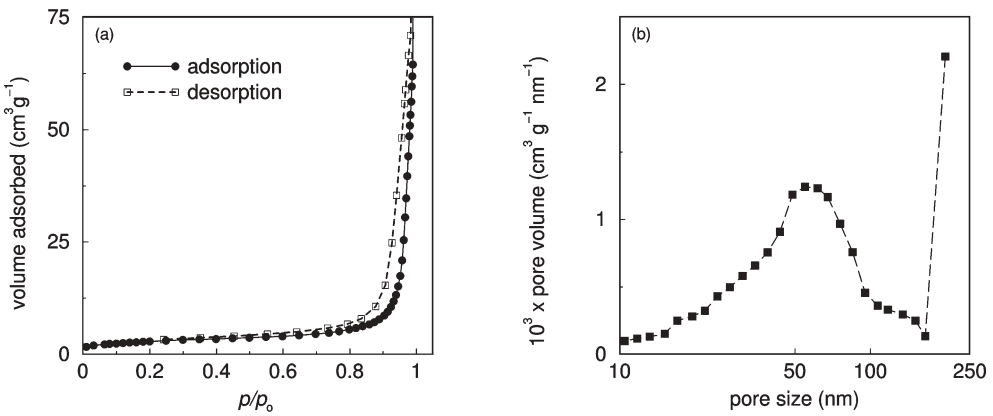

Fig. 11 (a) Nitrogen sorption isotherms of hierarchically porous MnO formed through reduction and vapour-phase leaching of macroporous $ZnMn_2O_4$ exhibit some hysteresis at high partial pressures. (b) A peak at 50 nm in the BJH pore size distribution agrees with our SEM and TEM observations. The macropores are too large to observe with nitrogen sorption, but the beginning of a second peak is visible at 250 nm.

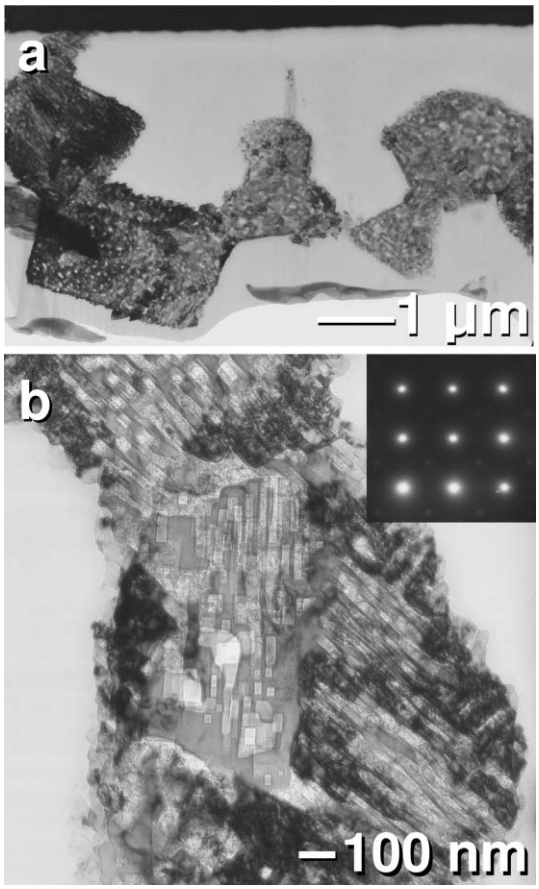

Fig. 12 (a) TEM micrograph of MnO/epoxy lamella formed with a focused ion beam. When seen at higher magnification, (b) the lamella has density variations due to the presence of pores. The region on the left has been tilted into the [100] zone axis (inset). Reproduced with permission from ref. 37. © 2006, American Chemical Society.

Conclusions

In this review, we have described how spontaneous processes based on solid-state reactivity can be controlled to give rise to unusual porous architectures. Subsequent reactions involving the resulting porous monoliths have led to conformal coatings, porous metals, and hierarchically porous structures. Slow solid-state kinetics can trap these architectures, leading to new possibilities for porous and biphasic materials. In particular, we find the formation of mesoporous single crystals through phase changes and vapor-phase leaching of a sacrificial element to be extremely intriguing. As these approaches are quite general, we hope that this work inspires further investigations into the formation of porous materials through template-free methods.

Acknowledgements

We gratefully acknowledge support from the National Science Foundation through a grant from the Chemical Bonding Center (CHE04-34567), through an IGERT award for E. S. T. (DGE99-87618), and for the use of MRSEC facilities (DMR05-20415). We also thank the Donors of the American Chemical Society Petroleum Research Fund for their support.

References

1 C. T. Kresge, M. Leonowicz, W. J. E. Roth, J. C. Vartuli and J. S. Beck, *Nature*, 1992, **359**, 710.
2 D. Zhao, J. Feng, Q. Huo, N. Melosh, G. H. Fredrickson, B. F. Chmelka and G. D. Stucky, *Science*, 1998, **279**, 548.
3 B. T. Holland, C. F. Blanford and A. Stein, *Science*, 1998, **281**, 538.
4 S. D. Sims, D. Walsh and S. Mann, *Adv. Mater.*, 1998, **10**, 151.
5 A. Imhof and D. Pine, *Nature*, 1997, **389**, 948.
6 G. Donnay and D. L. Pawson, *Science*, 1969, **166**, 1147.
7 R. J. Park and F. C. Meldrum, *J. Mater. Chem.*, 2004, **14**, 2291.
8 E. Loste, R. J. Park, J. Warren and F. C. Meldrum, *Adv. Funct. Mater.*, 2004, **14**, 1211.
9 J. Aizenberg, D. A. Muller, J. L. Grazul and D. R. Hamann, *Science*, 2003, **299**, 1205.
10 W. Yue, A. N. Kulak and F. C. Meldrum, *J. Mater. Chem.*, 2006, **16**, 408.
11 Y. –H. Ha, R. A. Vaia, W. F. Lynn, J. P. Constantino, J. Shin, A. B. Smith, P. T. Matsudaira and E. L. Thomas, *Adv. Mater.*, 2004, **16**, 1091.
12 P. Yang, T. Deng, D. Zhao, P. Feng, D. Pine, B. Chmelka, G. Whitesides and G. D. Stucky, *Science*, 1998, **282**, 2244.
13 B. T. Holland, L. Abrams and A. Stein, *J. Am. Chem. Soc.*, 1999, **121**, 4308.
14 M. W. Anderson, S. M. Holmes, N. Hanif and C. S. Cundy, *Angew. Chem., Int. Ed.*, 2000, **39**, 2707.
15 W. Deng and B. H. Shanks, *Chem. Mater.*, 2005, **17**, 3092.
16 B.-L. Su, A. Léonard and Z.-Y. Yuan, *C. R. Chim.*, 2005, **8**, 713.
17 H. Zhang and A. I. Cooper, *Ind. Eng. Chem. Res.*, 2005, **44**, 8707.
18 Y. Suzuki, N. Kondo and T. Ohji, *J. Am. Ceram. Soc.*, 2003, **86**, 1128.
19 R. S. Singh, C. A. Grimes and E. C. Dickey, *Mater. Res. Innovat.*, 2002, **4**, 178.
20 M. Raney, *US Pat.*, 1,563,787, 1925.
21 J. Erlebacher, M. J. Aziz, A. Karma, N. Dimitrov and K. Sieradzki, *Nature*, 2001, **410**, 450.
22 Y. Suzuki, T. Yamada, S. Sakakibara and T. Ohji, *Ceram. Eng. Sci. Proc.*, 2000, **21**, 19.
23 P. Levitz, G. Ehret, S. K. Sinha and J. M. Drake, *J. Chem. Phys.*, 1991, **95**, 6151.
24 H. Kim, M. Da Rosa, C. Boaro, J. Vohs and R. Gorte, *J. Am. Ceram. Soc.*, 2002, **85**, 1473.
25 R. Newnham, D. Skinner and L. Cross, *Mater. Res. Bull.*, 1978, **13**, 525.
26 M. Rajamathi, S. Thimmaiah, P. E. D. Morgan and R. Seshadri, *J. Mater. Chem.*, 2001, **11**, 2489.
27 M. Panda, M. Rajamathi and R. Seshadri, *Chem. Mater.*, 2002, **14**, 4762.
28 E. S. Toberer, A. Joshi and R. Seshadri, *Chem. Mater.*, 2005, **17**, 2142.
29 S. Hilpert and A. Wille, *Z. Phys. Chem.*, 1932, **18B**, 291.
30 J. B. Wiley and R. B. Kaner, *Science*, 1992, **255**, 1093.
31 C. H. Wallace, T. K. Reynolds and R. B. Kaner, *Chem. Mater.*, 1999, **11**, 2299.
32 M. Panda, R. Seshadri and J. Gopalakrishnan, *Chem. Mater.*, 2003, **15**, 1554.
33 E. S. Toberer, J. C. Weaver, K. Ramesha and R. Seshadri, *Chem. Mater.*, 2004, **16**, 2194.
34 T. K. Mandal and J. Gopalakrishnan, *J. Mater. Chem.*, 2004, **14**, 1273.
35 E. S. Toberer, T. D. Schladt and R. Seshadri, *J. Am. Chem. Soc.*, 2006, **128**, 1462.
36 E. S Toberer and R. Seshadri, *Adv. Mater.*, 2005, **17**, 2244.
37 E. S. Toberer, J. P. Löfvander and R. Seshadri, *Chem. Mater.*, 2006, **18**, 1047.
38 V. V. Doan and M. J. Sailor, *Science*, 1992, **256**, 1791.